16TH EUROPEAN CONFERENCE ON EARTHQUAKE ENGINEERING THESSALONIKI 18 - 21 JUNE 2018

SPATIAL VARIABILITY OF NEAR-FAULT EARTHQUAKE GROUND MOTION FROM 3D PHYSICS-BASED NUMERICAL SIMULATIONS

Chiara SMERZINI[1]

ABSTRACT

The evaluation of spatial variability of earthquake ground motion is crucial for the seismic analysis of spatially extended structures, such as bridges, viaducts and pipelines. However, observations at dense seismic arrays are still very scarce even on a worldwide scale especially in the near field region of large earthquakes and further investigations are needed. 3D physics-based numerical simulations of earthquake ground motion offer a powerful tool to simulate spatially variable ground motions, which can supplement observations when recorded data are lacking. The main aim of this paper is to evaluate the spatial variability of ground motions using the results of a wide set of 3D physics-based numerical simulations, with emphasis on near-fault conditions. The numerical dataset includes earthquake ground motion scenarios in different areas worldwide, namely, in the Po Plain and Marsica region (Italy), in Santiago (Chile) and in Wellington (New Zealand), with moment magnitude M_W between 6 and 7 and epicentral distance less than 30 km. For each case study, lagged coherency estimates are provided for both horizontal (fault-normal and fault-parallel) and vertical components of motion based on a standard spectral analysis and, then, are compared with the semi-empirical and empirical models available in the literature. To better identify the physical aspects underlying the spatial variability of motion, the dependence of coherency estimates on a variety of parameters, such as magnitude, source-to-distance, azimuth, fault-normal vs fault-parallel components, horizontal vs vertical components, site conditions, is presented and discussed.

Keywords: spatial variability of ground motion; lagged coherency; 3D physics-based numerical simulations; near-fault effects

1. INTRODUCTION

Earthquake ground motion exhibits spatial variability effects not only at a regional scale but also at local scales, with potential impact for the class of spatially extended structures. As a matter of fact, the largest dimension of most structures is usually small enough that the ground motion can be reasonably assumed to be the same at each point of the structure itself. On the other hand, for structures which extend over significant distances, such as bridges, viaducts and pipelines, ground motions arriving at different points of the structure may vary significantly both in amplitude and phase. In such cases evaluation of spatial variability of earthquake ground motion (SVEGM) is crucial to accurately estimate the structural seismic response and, referring to the design and assessment of bridges, a spatially varying seismic action has to be taken into account according to the 2008 Italian Building Code, NTC08 (CS.LL.PP., 2008) and to Eurocode 8, EC8 – Part 2 (CEN, 2005). According to EC8, the model describing the spatial variability of seismic actions should take into account, even if only in a simplified way, the propagative character of the seismic waves as well as the loss of correlation between motions at different points along the bridge owing to random heterogeneities of the soil and to differences in the mechanical properties of the involved media. Therefore, a good understanding of the physical factors underlying the SVEGM is of paramount relevance for the definition of an appropriate model for the variability of seismic input to be applied for the structural analysis of bridges.

[1]Department of Civil and Environmental Engineering, Politecnico di Milano, Italy, chiara.smerzini@polimi.it

Engineering models of SVEGM are usually calibrated from strong-motion dense array data from past earthquakes and neglect the issues related to the proximity to the seismic source. Several models of spatial coherency functions, both theoretical and empirical, have been developed on the basis of spectral estimation of the recorded data and regression fitting of an analytical function to the empirical coherency estimates (see e.g. Harichandran and Vanmarcke, 1986; Abrahamson et al., 1991a; 1991b; Luco and Wong, 1986; Ancheta et al., 2011). However, in spite of the increasing availability of strong motion records, observations at dense arrays are still very scarce even on a worldwide scale, especially in near-source conditions scale.

As an alternative powerful method, numerical simulations of earthquake ground, based on physical models of the seismic source, the propagation path from the source to the site and local geologic irregularities, can be used to simulate spatially variable ground motion when recorded data are lacking. The main aim of this paper is to evaluate the spatial variability of ground motions using the results of a wide set of 3D physics-based numerical simulations, with emphasis on near-fault conditions. Note that this approach has the great advantage of allowing one to investigate the dependence of SVEGM on physical factors, such as magnitude, near-source effects, local site conditions, for a variety of "virtual", albeit realistic, conditions. The numerical dataset includes earthquake ground motion scenarios in different areas worldwide, namely, in the Po Plain and Marsica region (Italy), in Santiago (Chile) and in Wellington (New Zealand), with moment magnitude M_W between 6 and 7 and epicentral distance R_{epi} < 30 km. The numerical results are obtained using the high-performance computer code SPEED (http://speed.mox.polimi.it), based on the Discontinuous Galerkin Spectral Element method (Mazzieri et al., 2013).

For each case study, lagged coherency estimates are provided for both horizontal (fault-normal and fault-parallel) and vertical components of motion based on a standard spectral analysis and, then, are compared with the semi-empirical and empirical models available in the literature. To better identify the physical aspects underlying the spatial variability of motion, the dependence of coherency estimates on a variety of parameters, such as magnitude, source-to-distance, azimuth, fault-normal vs fault-parallel components, horizontal vs vertical components, site conditions, is presented and discussed.

2. OVERVIEW ON SPATIAL VARIABILITY OF EARTHQUAKE GROUND MOTION

2.1 Theoretical background

The importance of SVEGM has been recognized for a long time in earthquake-resistant design and analysis of large and extended structures and is associated with three different factors (see e.g. Kramer, 1996; Harichandran, 1999):

(i) wave passage effect, arising from differences in the arrival times of seismic waves at separate stations on ground surface;
(ii) extended source and ray-path effects, arising from differences in the manner of superposition of waves (a) arriving from an extended source, especially in the near-source region, and (b) scattered by irregularities and heterogeneities along the path from the source to the site;
(iii) local site effects, arising from differences in local sub-surface soil conditions at each station, which may alter the amplitude and frequency content of seismic waves propagating from the bedrock to the ground surface.

The common approach to quantify SVEGM in engineering applications is the evaluation of the spatial coherency function (for a thorough overview see Zerva, 2009). The coherency of the seismic motions is obtained from the cross spectral density of the time histories between two sites, normalized with respect to the corresponding power spectral density. More specifically, given a pair of motions recorded at two discrete locations j and k at a separation distance d, the coherency $\gamma_{jk}(\omega,d)$, function of both circular frequency ω (or frequency f, with $\omega = 2\pi f$) and distance (d), can be computed as follows:

$$\gamma_{jk}(\omega,d) = \frac{S_{jk}(\omega,d)}{\sqrt{S_{jj}(\omega)\cdot S_{kk}(\omega)}} \tag{1}$$

where:

$S_{jj}(\omega)$ and $S_{kk}(\omega)$ are the smoothed power spectral density at stations j and k, respectively, defined as the Fourier transform of the auto covariance function of the two signals, $C_{kk}(t)$ and $C_{jj}(t)$;

- $S_{jk}(\omega,d)$ is the smoothed cross spectrum between stations j and k, defined as the Fourier transform of the cross covariance function, $C_{jk}(t)$, between stations j and k.

The coherency function of Eq.(1) is a complex function and can be therefore expressed as follows:

$$\gamma_{jk}(\omega,d) = \left|\gamma_{jk}(\omega,d)\right| \cdot exp\left[-i\theta_{jk}(\omega,d)\right] \tag{2}$$

where $|\gamma_{jk}(\omega,d)|$, termed lagged coherency (note that $0 \leq |\gamma_{jk}(\omega,d)| \leq 1$), is the absolute value and $\theta_{jk}(\omega,d)$ is the phase spectrum. The lagged coherency and is the most commonly used coherency measure in engineering applications and it provides, at each frequency f, the degree of "similarity" of earthquake ground motions, i.e., the extent to which data recorded by two stations at distance d are correlated. It is expected that at small separation distances and at low frequencies motions are highly correlated and, therefore, the lagged coherency will tend to unity for d or f approaching zero. On the other hand, at large separation distances and at high frequencies, motions tend to be completely uncorrelated and, therefore, theoretically, the lagged coherency will tend to zero for large values of d or f.

2.2 Engineering models of spatial coherency

A variety of spatial coherency models has been developed on the basis of the spectral estimation of recorded data and regression fitting of an analytical function to the empirical coherency estimates. There are two main classes of coherency models: semi-empirical and empirical models. The semi-empirical models differ from the empirical ones as they provide functional forms obtained from analytical derivations, where model parameters require calibration from recorded data. Examples of semi-empirical models are: Luco and Wong (1986), Somerville et al. (1988), Der Kiureghian (1996) and Zerva and Harada (1997). Among these studies, one of the most widely used models in engineering applications is the Luco and Wong (1986) model, referred to hereafter as LW86. It is based on the analysis of shear waves propagating through random media and gives the following expression for the lagged coherency:

$$\left|\gamma(\omega,d)\right| = \cdot exp[-(\alpha \cdot \omega \cdot d)^2] \tag{3}$$

where α is the coherency drop parameter controlling the exponential decay of the coherency with distance and frequency; increasing values of α implies a higher decay of coherency as d and ω increase. A median value of α equal to $2.5 \cdot 10^{-4}$ s/m is suggested by the authors. The functional form of Eq. (3) will be largely used in this work.

The development of empirical models began with the analysis of the first seismic data recorded at the Strong Motion Array - Phase 1 (SMART-1), located at Lotung, Taiwan, in an alluvial valley. The SMART-1 array is a two-dimensional surface array consisting of 37 stations arranged in three concentric circles with a minimum spacing of 100 m. Relying on SMART-1 array data, various researchers proposed empirical model for lagged coherency, such as Loh (1985), Harichandran and Vanmarcke (1986), Oliveira et al. (1991), Abrahamson et al. (1991a; 1991b) and Ancheta et al. (2011). In EPRI (2006; 2007) a spatial coherency model, derived from the analysis of different dense arrays worldwide, was proposed.

3. ESTIMATING SPATIAL COHERENCY FROM 3D PHYSICS-BASED NUMERICAL SIMULATIONS

In this work, spatial coherency estimates are obtained using 3D physics-based numerical simulations of earthquake shaking through the spectral element code SPEED (Mazzieri et al. 2013). Deterministic approaches, like the spectral element method adopted in this study, rely on the rigorous numerical

solution of the seismic wave propagation problem and can provide synthetic ground motion time histories consistent with the 3D model of the seismic source, of the source-to-site propagation path and of local site response.
This numerical approach has the following main advantages:

(i) possibility to locate an arbitrary number of receivers at the desired locations, with the desired inter-station distances and at desired soil conditions (soft/stiff soil vs rock);
(ii) generation of arbitrary earthquake scenarios with prescribed magnitude at a given source-to-site distance, giving the possibility to study near-source motions;
(iii) possibility to investigate the physical mechanisms underlying the SVEGM in a more systematic way than empirical models can do owing to the lack of data;
(iv) finally, application of homogeneous spectral processing techniques, avoiding the inevitable issues related to the subjectivity in the numerical processing of data from different arrays and during different events.

On the other hand, the main drawback of 3D physics-based numerical simulations is the frequency threshold of computed results, hardly larger than about 2 Hz, and the related limit in the minimum spacing between mesh nodes.

3.1 Case studies

As a numerical dataset, 3D physics-based synthetic motions obtained at dense arrays in different areas worldwide are used, as provided in Table 1. Figure 1 shows the location of the dense networks for the case studies under consideration together with the surface projection of the causative faults and the epicenter location. Note that:

- for Marsica (Central Italy): the historical M_W 6.7 Jan 13 1915 earthquake together with a smaller (M_W 6.0) hypothetical earthquake, originating from the same normal fault, and three arrays (two inside the soft basin, A1÷A2, soil class C/D with shear wave velocity at ground surface V_S = 180 m/s and one on outcropping bedrock with V_S = 1000 m/s) are taken into account;
- for Emilia (Northern Italy): only the M_W 6.0 May 29 2012 earthquake, with reverse focal mechanism, and 4 different arrays (A1÷A4) in the Po Plain (soil class C with V_S = 300 m/s), are considered;
- for Wellington (New Zealand): three hypothetical earthquake scenarios originating from a strike-slip fault, with M_W = 6.0, 6.5 and 7.0, and two arrays (A1÷A2) in the Wellington bay area (soil class C with V_S = 300 m/s), are considered;
- for Santiago (Chile): three hypothetical earthquakes scenarios, with M_W = 6.0, 6.5 and 6.7, originating from the reverse San Ramon fault bordering the Eastern edge of Santiago basin, and two arrays (A1 inside the basin – soil class B with V_S = 400 m/s and A2 on rock with V_S = 2400 m/s), are simulated.

Table 1. List of 3D numerical simulations used for the estimation of SVEGM.

Location	**Arrays**	**EC8 site class**	**Earthquake Scenario**	**Fault Type**	**M_W**	**f_{max} (Hz)**	**References**
Marsica, Central Italy	A1÷A3	A1÷A2: C/D A3: A	Hypothetical Jan 13 1915	Normal	6.0 6.7	2.0	Paolucci et al. (2016)
Emilia, Northern Italy	A1÷A4	A1÷A4: C	May 29, 2012	Reverse	6.0	1.5	Paolucci et al. (2015)
Wellington, New Zealand	A1÷A2	A1÷A2: C	Hypothetical	Strike-slip	6.0 6.5 7.0	2.0	Paolucci et al. (2014)
Santiago, Chile	A1÷A2	A1: B A2: A	Hypothetical	Reverse	6.0 6.5 6.7	2.0	Paolucci et al. (2014)

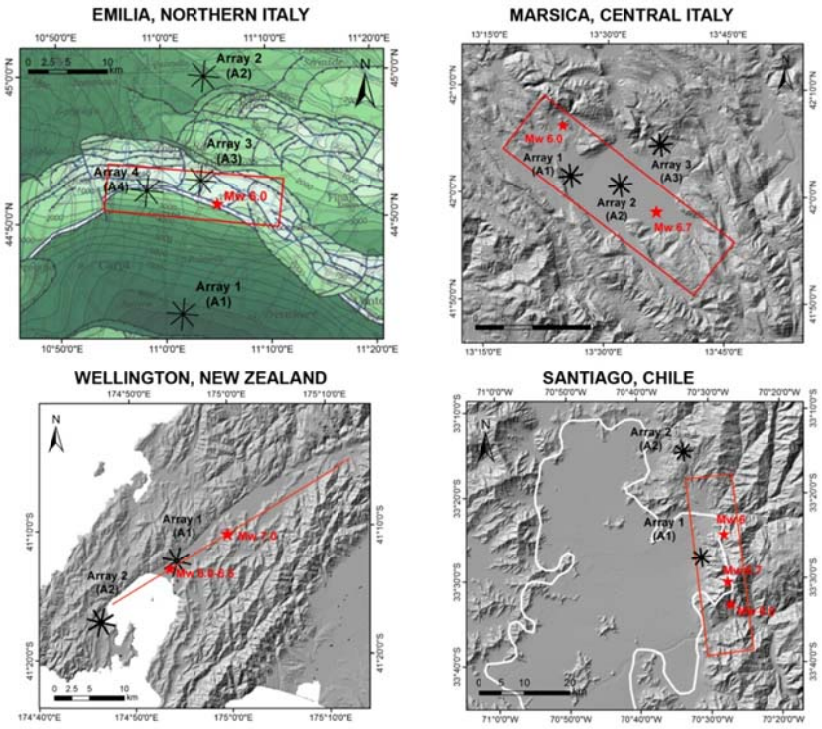

Figure 1. Sketch of the dense arrays used to estimate spatial coherency from 3D physics-based numerical simulations: (1) Emilia, Northern Italy (top left); (2) Marsica, Central Italy (top right); (3) Wellington, New Zealand (bottom left); (4) Santiago, Chile (bottom right). See also Table 1.

3.2 Procedure

Estimation of spatial coherency is carried out through a spectral analysis in the frequency domain according to the following procedure (for further details the reader is referred to Zerva 2009):

(1) a pair of stations located at separation distance d is selected; the center point of the array is selected as reference station and is maintained fixed;
(2) the simulated time histories are aligned to remove the wave passage effects by shifting the time axis of a time history with respect to the reference station by an amount corresponding to the time lag associated to the peak of the cross covariance function;
(3) nearly-stationary segments of the time series, containing the strongest phase of shaking, are selected, they are computed as the portion of the signal associated with values of the normalized Arias Intensity, I_a, between 5% and 80%;
(4) a Tukey (tapered cosine) window with tapering length equal to 5% of the length of stationary part of the signal is then applied to the time history;
(5) from the windowed and tapered time signals, the power and cross spectra are calculated;
(6) a Hamming spectral window of width equal to 0.5 Hz (the length M is then determined *a posteriori* to have this prescribed frequency bandwidth) is used to smooth the power and cross spectra;
(7) the complex valued coherency is estimated using Eq. (1) and, then, the lagged coherency is derived.

The issue of smoothing of the spectral estimators (point 6) is crucial for extracting meaningful information regarding the coherency of the signals and has a considerable impact on results. Abrahamson et al. (1991b), in evaluating an optimal window for the estimation of the coherency, suggested an 11-point (M=5, being N=2M+1 the number of points of the smoothing window) Hamming (spectral) window, if the coherency estimate is derived from time windows less than approximately 2000 samples and is to be used in structural engineering applications, with damping coefficient 5% of critical. The criterion adopted in this study is consistent with the Abrahamson's recommendations, as it implies the use of a 11-point (M=5) Hamming window for time histories less

than 2048 samples, while a 21-point (M=10) window is adopted for longer signals.
Since synthetic ground motions are in the near-field region of moderate to severe earthquakes, where source directivity/directionality effects may be predominant and lead to polarization of ground motion in the strike normal and parallel directions, the two horizontal components projected along the direction parallel and normal to the fault strike (FP = Fault Parallel and FN = Fault Normal, respectively), are taken into consideration. In the following results will be, in fact, discussed in terms of FP, FN and vertical (UD) coherency estimates.

4. SPATIAL COHERENCY ESTIMATES

Estimates of lagged spatial coherency $|\gamma|$ are provided in this section on the basis of the procedure described previously, for the different cases studies under consideration. In the following reference is made only to the lagged coherency so that the term lagged will be omitted. Inter-station distances in the range 0-1000 m are considered and are grouped in ten 100-m bins, with each bin represented by the average distance of the station pairs belonging to it. The size of the distance bin (100m) is dictated mainly by the minimum size of the elements of the meshes. Note that the coherency estimates are limited to a relatively small frequency interval, being the maximum frequency of the numerical models in the range 1.5-2 Hz. For this reason, a common frequency axis between 0 and 2 Hz will be adopted in the following for graphical purposes.
As an illustrative example, Figure 2 shows the results for the Marsica scenario (Mw=6.7), Array A1: the individual coherency curves associated with each pair of stations (thin grey line) along with the mean curve (black thick line) for the FP component of ground computed. Results obtained from the 3D physics-based synthetics are compared with: (i) the LW86 model of Eq. (3) with $\alpha = 2.5 \cdot 10^{-4}$ s/m, as suggested by the authors (magenta line); and (ii) the empirical model by Harichandran and Vanmarcke (1986), referred to as HV86 (green line). These models are computed considering the average distance of each distance bin, reported in the title of each subplot. Note that LW86 is a semi-empirical model, therefore the parameter α should not be fixed *a-priori* but calibrated on the synthetic dataset by least-squares fitting.

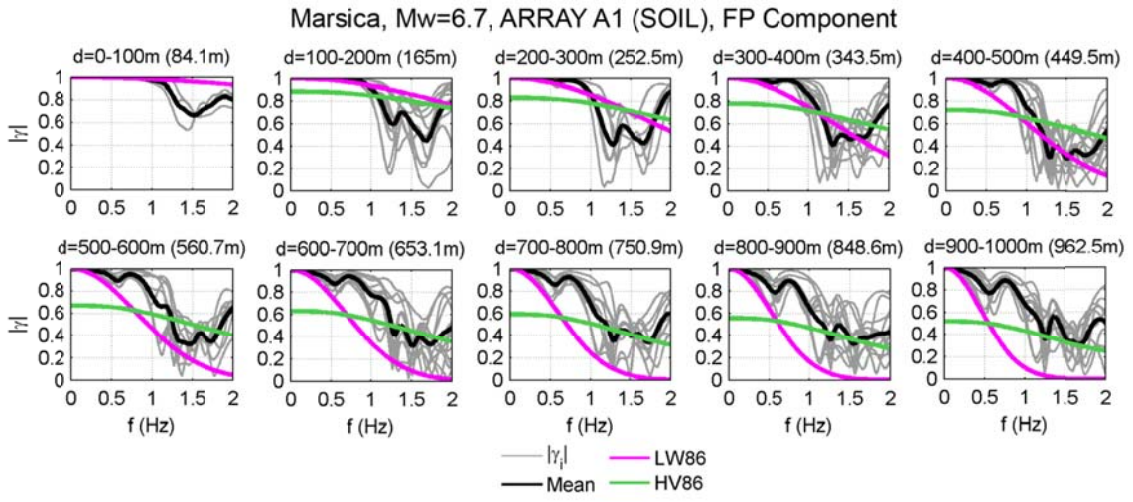

Figure 2. Marsica (Mw=6.7), Array A1 (soil): lagged coherency estimates of FP component of ground motion as a function of frequency (0-2 Hz), for 100-m distance in the interval 0-1000 m. Note: LW86=Luco and Wong (1986) for $\alpha=2.5 \cdot 10^{-4}$ s/m; HV86 = Harichandran and Vanmarcke (1986).

Given the variety of case studies considered in this work and the multiplicity of variables on which the lagged coherency depends, it is helpful to find a concise measure of spatial coherency, apt for identifying common trends and performing some statistics. To this end, the value of the coherency drop parameter α of LW86 model is computed by non-linear least-squares regression of the coherency estimates for each distance bin and ground motion component.
Figure 3 shows the best fitting α values as a function of distance, separately for the three ground

motion components, FP (black line), FN (red line) and UD (blue line), and for soil (continuous line) and rock (dashed line) conditions, for the set of M_W=6 scenarios under study. Decay of fitted α with frequency has not been analyzed herein owing to the relatively small frequency range of the numerical simulations. Note that the plotted values of fitted α are multiplied by a 10^4 factor and represented in Log_{10} scale to better appreciate their variability. Results indicate a strong non-linear dependence of α on distance: α turns out to decrease with increasing inter-station distance at a rate which tends to be higher at smaller distances. Similar conclusions were derived in the recent work by Konakli et al. (2014), on the basis of the analysis of strong-motion recordings the UPSAR array during the Mw=6 Parkfield earthquake in California. Furthermore, fitted α shows a rather large variability taking values in the ranges: ~ $8{\cdot}10^{-5} \div 2{\cdot}10^{-3}$, for Marsica; ~ $4{\cdot}10^{-5} \div 1{\cdot}10^{-3}$, for Emilia; ~ $6{\cdot}10^{-5} \div 8{\cdot}10^{-4}$, for Wellington; ~ $7{\cdot}10^{-6} \div 3{\cdot}10^{-4}$, for Santiago. Note that very high coherency estimates, corresponding to low values of α, are systematically found at Santiago arrays, especially for Mw=6 and rock conditions, most likely due to effects related to the particular source-receiver configuration and the large velocities on outcropping bedrock (V_S=2400 m/s). If we exclude the latter case study, α values show a reasonable range of variability, from about $5{\cdot}10^{-5}$ to $2{\cdot}10^{-3}$, in substantial agreement with the range found by Konakli et al. (2014) for Parkfield recordings at UPSAR array (~$6{\cdot}10^{-5} \div 10^{-3}$).
The dependence of fitted α on a series of physical parameters, such as ground conditions (soft soil vs rock), ground motion component (FN vs FP vs UD), magnitude, source-to-site distance and azimuth, will be discussed in the following sections.

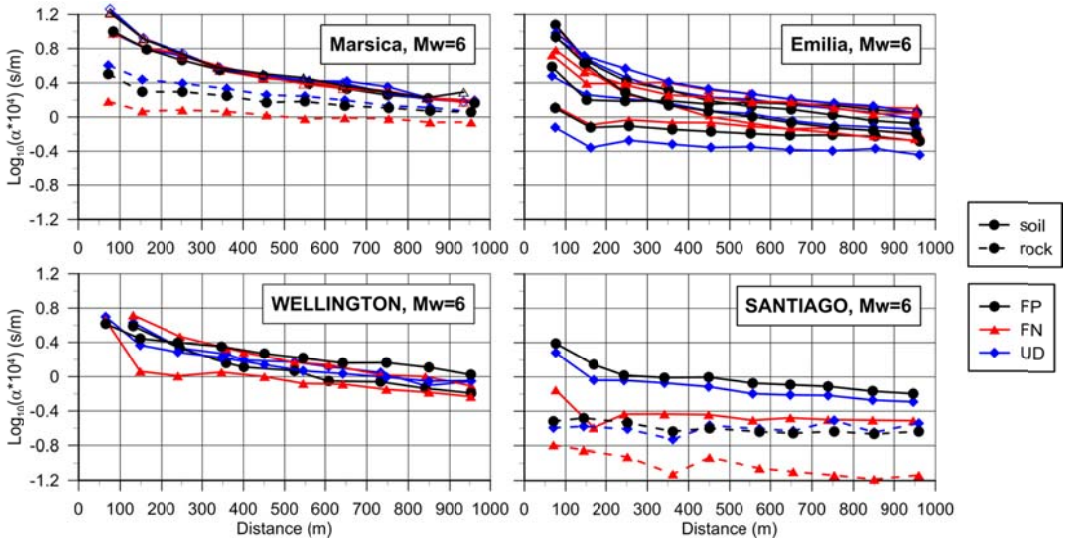

Figure 3. Best fitting α values of LW86 model as a function of separation distance for FP (black), FN (red) and UD (blue) components, both on soft sediments (solid line) and on outcropping bedrock (dashed lines), for the set of Mw=6 scenarios under study.

4.1 Dependence on magnitude

From a theoretical point of view, a reduction of coherency for large magnitudes in near-field should be expected with respect to small magnitude events owing to the increase of the variability of wave paths involving different portions of the fault rupture. Figure 4 illustrates the magnitude dependence of the best fitting α values considering the dense arrays on rock conditions (Marsica and Santiago case studies). Results for the three ground motion components, FN, FP and UD, are reported.
The results for the Marsica case study suggest a higher spatial coherency (i.e., smaller α values) for the larger earthquake (Mw=6.7 vs Mw=6), at all separation distances, at least in the considered range of frequencies. This effect is found also on soft soil sites (not shown herein for brevity), in agreement with the findings of Abrahamson et al. (1991a), who found that small magnitude events have lower coherency than large magnitude events in the range of frequency below 5 Hz, on the basis of strong motion recordings. However, the other case studies do not confirm this positive correlation between

magnitude and coherency. Referring to the Santiago case, a reverse trend is found: coherency of the smallest earthquake turns out to be larger than that of the strongest earthquake at all separation distances and for all ground conditions. A similar behavior was found also for Wellington case study. Further case studies should be analyzed to draw more general conclusions. It should be also noted that for these simulations the differences in earthquake magnitude are rather limited, being equal to 1 magnitude point at most. Consideration of scenarios characterized by very different magnitude (e.g. Mw=7 vs Mw=5) could help clarify this aspect.
It is worth remarking that this ambiguity regarding the effect of magnitude on spatial coherency is found also in the literature. Contrarily to Abrahamson et al. (1991a), Somerville et al. (1988) suggested that coherency for aftershocks is greater at all frequencies than that for mainshock in the near-field region. This was also confirmed, more recently, by the results of AfifChaouch et al. (2016) using simulations by means of the Empirical/Hybrid Green Function (H/EGF) techniques.

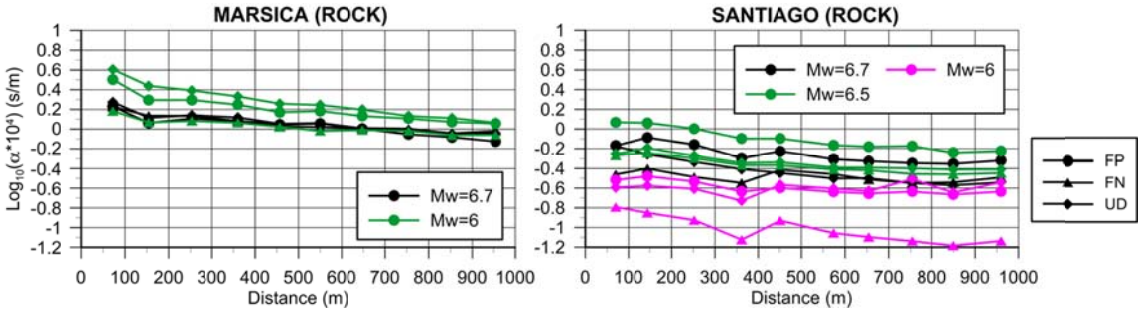

Figure 4. Magnitude dependence of best fitting α values on soil conditions, for Marsica (left) and Santiago (right) case studies.

4.2 Dependence on source-to-site distance

The Emilia case study offers the possibility to investigate the effect of source-to-site distance on spatial coherency, even though the numerical model spans a limited range of epicentral distances, up to about 30 km. Figure 5 presents the best fitting α values (FP vs FN vs UD) as a function of separation distance for the four Emilia arrays, grouped into two sets: A3÷A4 (grey lines), located on the surface projection of the fault at Joyner-Boore (R_{JB}) distances equal to 0, and A1÷A2 (red lines), located farther from the fault at R_{JB} ~ 12 km.
It turns out that the proximity to the extended seismic source produces less coherent motion, as intuitively expected, owing to the extended source effect, and this effect is more significant at small separation distances. As a matter of fact, in the near-source region of an earthquake, wave packets radiating from different portion of the fault cause differential motion owing to the differences in relative geometry of the source and the sites, implying different azimuths, incidence angles and ray paths. Getting farther from the source, ground motion is less affected by the details of the finite-fault rupture and waves propagating from the fault tend to arrive almost synchronously at nearby stations. Note that the α values at Array A2 are smaller than those at Array A1 for any distance, implying a loss of coherency at A2 with respect to A1. This can be easily explained as a combination of source directivity and local site effect, as A2 is located in the region strongly affected by forward up-dip directivity effects and by the propagation of surface waves, generated by the buried morphological irregularity of the Mirandola structural high (see Paolucci et al., 2015 for further details).
These results are in substantial agreement with previous studies based both on ground motion recordings (Abrahamson et al. 1991a; Somerville et al. 1988) and deterministic numerical modelling (AfifChaouch et al., 2016).

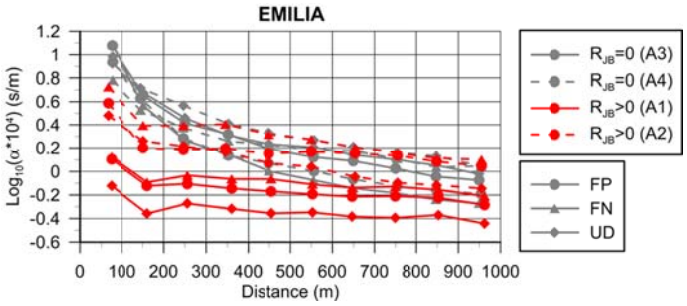

Figure 5. Source-to-site distance dependence of best fitting α values for the Emilia case study: grey lines refer to arrays located on the surface projection of the fault (R_{JB}=0), while red lines correspond to more distant arrays with R_{JB}~12 km.

4.3 Dependence on soil conditions

Figure 6 illustrates the effect of site condition on spatial coherency with reference to the Marsica case study (Mw=6.7): the best fitting α values obtained for the station pairs located on soft/stiff sites are compared with those derived for the stations on outcropping bedrock, for the three ground motion components. Consider that Marsica soil sites (Arrays A1 and A2) are located within the very soft alluvium basin with superficial V_S=180 m/s, while rock sites (Array A3) is characterized by V_S ~1000 m/s. In agreement with literature studies (Abrahamson et al., 1991a; EPRI, 2007; AfifChaouch et al., 2016), it turns out that, for all ground motion components, spatial coherency on soft soils can be significantly lower than that on rock, owing to the influence of local subsurface irregularities which modify the amplitude and frequency content of incident waves. Such an effect seems to be more pronounced at small separation distances, whereas it decreases at larger separation distances.

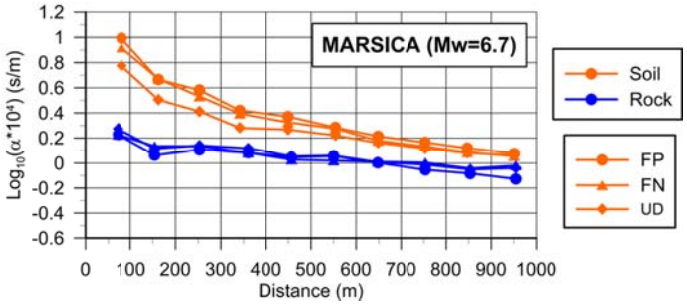

Figure 6. Site condition dependence of best fitting α values for the Marsica case studies (Mw=6.7): orange lines refer to soil sites, while blue lines refer to rock sites.

4.4 Dependence on ground motion component

To study the dependence of coherency on ground motion components, the ratios α_{FN}/α_{FP}, α_{FN}/α_{UD} and α_{FP}/α_{UD}, with α_{FN} (or α_{FN} or α_{UD}) representing the fitted α value on the FN (or FP or UD) component, have been computed for each distance bin and for each case study. All station pairs located on soft/stiff soil conditions have been grouped together and processed homogeneously to find a curve common to all soil sites. Then, the average of the ratios α_{FP}/α_{UD} and α_{FN}/α_{UD}, denoted by α_H/α_{UD}, has been calculated to provide a measure of the relationship between horizontal and vertical coherency.
Figure 7 presents the ratios α_{FN}/α_{FP} (left) and α_H/α_{UD} (right), subdivided into two sets of data with homogenous magnitude, Mw=6 (top panel) and Mw=6.5-6.7 (bottom panel). Note that, in general, a value of the ratio α_a/α_b less (or larger) than 1 means that the coherency for component "*a*" is larger (smaller) than that for component "*b*".
It can be noted that:

- α_{FN}/α_{FP} tends to be smaller than 1, i.e., coherency of FN component is larger than that of FP component, for all receivers on soft/stiff soil and rock, most likely because near-field motion

tend to polarize along the direction perpendicular to fault strike owing to the synchronous arrival of waves radiated by the fault. A clear exception to this trend is represented by the Emilia case study, where the condition $\alpha_{FN}/\alpha_{FP} < 1$ holds only for Array A3, affected by strong up-dip directivity effects, while a reverse trend is found at remaining arrays. This may be due to the fact that the FN component corresponds to the direction where complex site effects, associated with the propagation of prominent trains of surface waves, control earthquake ground motion and, hence, may induced a significant loss of coherency.

- for the lower magnitude set, α_H/α_{UD} tends to be smaller than 1, i.e., coherency of horizontal components is larger than that of vertical component, for all considered case studies, apart from slight deviations. A reverse trend is typically found for larger magnitude events, especially at small to intermediate separation distances, with ratios α_H/α_{UD} varying between 0.8 and 1.5. This may be interpreted in light of the fact that, for more severe earthquakes, the rupture involves a significantly larger portion of the fault, implying a larger variability in terms of source-to-site relative geometry and rupture propagation and, thus, a loss of coherency. Such an increase of incoherency is expected to affect predominantly horizontal components, owing to the smaller velocities of S waves together with the occurrence of site effects.
- No clear trend with focal mechanism is found, although for strike-slip events (Wellington) a trend with $\alpha_{FN}/\alpha_{FP} < 1$ and $\alpha_H/\alpha_{UD} > 1$ is found.

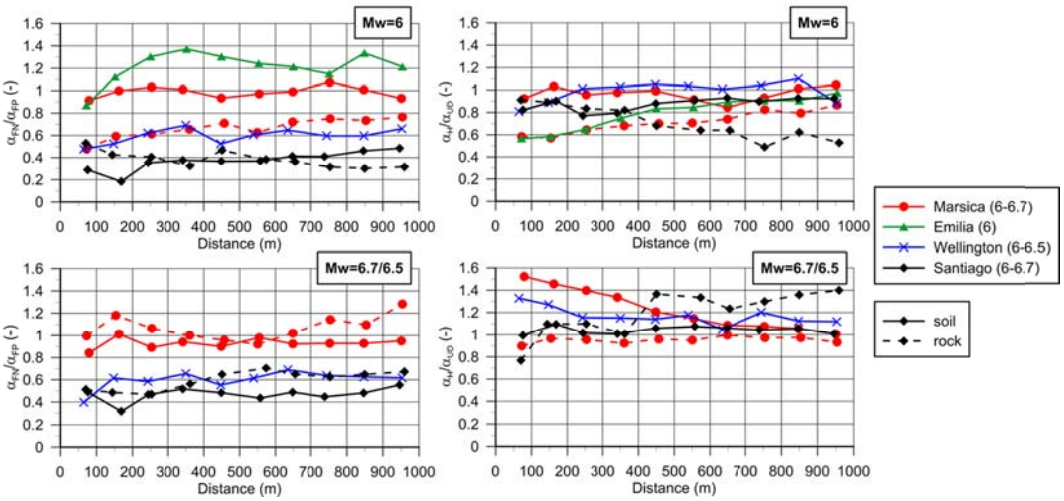

Figure 7. Ratios α_{FN}/α_{FP} (left) and α_H/α_{UD} (right) for both soft/stiff soil (continuous lines) and rock conditions (dashed lines) for two homogeneous magnitude sets, Mw=6 (top panel) and Mw=6.5-6.7 (bottom panel).

5. CONCLUSIONS

Owing to the substantial lack of earthquake recordings at closely spaced stations, there are still aspects related to the SVEGM that deserve further investigations, especially when characterization of ground motion in the near source region of severe earthquakes is of concern. In this study, 3D physics-based numerical simulations of earthquake ground, including a 3D model of the seismic wave propagation phenomenon from the fault rupture up to the site of interest, have been used to generate ground motions at closely spaced sites in different areas worldwide (Po Plain, Northern Italy; Marsica: Central Italy; Wellington, New Zealand; Santiago, Chile) and to estimate the spatial coherency for a range of conditions in terms of source parameters (magnitude, focal mechanism), source-to-site configuration (distance, azimuth, directivity effects) and site conditions (soft sites vs rock), with emphasis on the near-source region.

The most salient results of this work can be summarized as follows:

- in agreement with the results published by Konakli et al. (2014), the coherency drop parameter α shows a non-linear dependence with separation distance: it decreases with increasing distance at a rate which tends to be higher at smaller distances. Therefore, the assumption of a

constant value of α, as routinely done in engineering practice for the analysis and design of extended structures, should be evaluated with care;

- in conditions of proximity to the seismic source, spatial coherency tends to be smaller than that given by empirical models, especially at small separation distances, owing to the loss of coherency induced by the extended seismic source, directivity/directionality effects and propagation patterns in complex 3D geological structures, such as alluvial valleys;
- typically, coherency of FN component tends to be larger than that of FP component, regardless of magnitude and of site condition (soft/stiff soil or rock), because near-source motion polarizes along the direction perpendicular to fault strike owing to the synchronous arrival of waves radiated by the rupture wavefront;
- coherency of vertical motion, as compared to horizontal one, turns out to be magnitude dependent: for lower magnitudes, coherency of horizontal components tends to be larger than that of vertical component, while a reverse trend is found for larger earthquakes, especially at small to intermediate separation distances;
- a clear dependence on magnitude is not found: a loss of coherency for increasing magnitude is observed for the majority of case studies, as intuitively expected, but a reverse behavior is found for Marsica earthquakes. Such an ambiguity is most likely due to the interaction of different factors affecting ground shaking (slip pattern on the fault, source-to-site configurations, source-basin interaction) which cannot be easily distinguished in the synthetics. Note that contradictory findings are also reported in the literature (Abrahamson et al., 1991a; Somerville et al., 1988; EPRI, 2007; AfifChaouch et al., 2016);
- simulations confirm a strong dependence of coherency on site condition (soft/stiff soil vs rock): for all ground motion components, spatial coherency on soft soils can be significantly lower than that on rock, owing to the influence of local subsurface irregularities which modify the amplitude and frequency content of seismic waves.

Future work will extend the analysis to further case studies to confirm and better explain and the role played by some important physical factors, such as ground motion component, magnitude, source-to-site azimuth, on SVEGM.

6. ACKNOWLEDGMENTS

The work has been carried out in the framework of the 2014-2016 RELUIS Special Project RS2 "Numerical simulations of earthquakes and near-source effects" funded by the Italian Department of Civil Protection. The fruitful suggestions by Roberto Paolucci are greatly acknowledged.

7. REFERENCES

Abrahamson N.A., Schneider J.F., and Stepp J.C. (1990). Spatial variation of strong ground motion for use in soil-structure interaction analyses, *in Proc of 4th US-Natl Conf on Earthquake Engineering*, Palm Springs CA, 317–326.

Abrahamson N.A., Schneider J.F., and Stepp J.C. (1991a) Spatial coherency of shear waves from the Lotung, Taiwan large-scale seismic test. *Structural Safety*, 10:145–162

Abrahamson N.A., Schneider J.F., and Stepp J.C. (1991b). Empirical spatial coherency functions for application to soil-structure interaction analyses. *Earthquake Spectra* 7(1):1–27

AfifChaouch K., Tiliouine B., Hammoutene M., Rupakhety R., and Sigbjörnsson R. (2016), Estimating ground motion incoherence through finite source simulation: a case study of the 1980 El-Asnam earthquake. *Bulletin of Earthquake Engineering*, 14 (4): 1195-1217

Ancheta T.D., Stewart J.P., and Abrahamson N.A. (2011). Engineering characterization of earthquake ground motion coherency and amplitude variability. In *Proc. 4th IASPEI / IAEE International Symposium: Effects of Surface Geology on Seismic Motion*, University of California, Santa Barbara.

CEN, European Committee for Standardization (2005) Eurocode 8 - Design of structures for earthquake resistance - Part 2: Bridges.

CS.LL.PP. (2008). DM 14 Gennaio 2008. Norme tecniche per le costruzioni, Gazzetta Ufficiale della Repubblica Italiana, 29. (in Italian)

Der Kiureghian A. (1996). A coherency model for spatially varying ground motions. *Earthquake Engineering and Structural Dynamics*, 25: 99–111.

EPRI (2006). Program on technology innovation: Spatial coherency models for soil-structure interaction. Technical Update Report 1012968, EPRI.

EPRI (2007). Program on technology innovation: Effects of spatial incoherence on seismic ground motions. Technical Report 1015110, EPRI

Harichandran R.S. (1999). Spatial variation of earthquake ground motion. What is it, how do we model it, and what are its engineering implications?, Technical Report, Department of Civil and Environmental Engineering, Michigan State University.

Harichandran R.S., and Vanmarcke E. (1986). Stochastic variation of earthquake ground motion in space and time. *J Eng Mech* ASCE 112(2): 914–925

Konakli K., Der Kiureghian A., and Dreger D. (2014). Coherency analysis of accelerograms recorded by the UPSAR array during the 2004 Parkfield earthquake, Earthquake Engineering and Structural Dynamics, 43: 641-659

Kramer S.L. (1996) Geotechnical Earthquake Engineering, Prentice Hall College.

Loh C.H. (1985). Analysis of the spatial variation of seismic waves and ground movements from SMART-1 data. *Earthquake Engineering and Structural Dynamics*, 13, 561–581.

Luco J.E., and Wong H.L. (1986). Response of a rigid foundation to a spatially random ground motion. *Earthquake Engineering and Structural Dynamics*, 14: 891–908.

Mazzieri I., Stupazzini M., Guidotti R., and Smerzini C. (2013). SPEED-Spectral Elements in Elastodynamics with Discontinuous Galerkin: a non-conforming approach for 3D multi-scale problems. *International Journal for Numerical Methods in Engineering*, 95 (12): 991-1010.

Oliveira C.S., Hao H., and Penzien J. (1991). Ground motion modeling for multiple-input structural analysis. *Structural Safety*, 10: 79–93.

Paolucci R., Mazzieri I., Smerzini C. and Stupazzini M. (2014) Physics-based earthquake ground shaking in large urban areas, in *Perspectives on European Earthquake Engineering and Seismology, Second European Conference on Earthquake Engineering and Seismology*, vol. 34, chap. 10, pp. 331–359, ed. Ansal, A., Springer.

Paolucci R., Mazzieri I. and Smerzini C. (2015). Anatomy of strong ground motion: near-source records and 3D physics-based numerical simulations of the Mw 6.0 May 29 2012 Po Plain earthquake, Italy. *Geophysical Journal International*, 203: 2001-2020.

Paolucci R., Evangelista L., Mazzieri I., and Schiappapietra E. (2016). The 3D Numerical Simulation of Near-Source Ground Motion during the Marsica Earthquake, Central Italy, 100 years later. *Soil Dynamics and Earthquake Engineering*, 91: 39-52.

Somerville P.G., McLaren J.P., Saikia C.K. and Helmberger DV (1988) Site-specific estimation of spatial incoherence of strong ground motion, In *Proc. Earthquake Engineering and Soil Dynamics II, recent advances in ground-motion evaluation,* Geotechnical Special Pub No 20 ASCE, Park City, Utah, pp 188–202.

Zerva A., and Harada T. (1997). Effect of surface layer stochasticity on seismic ground motion coherence and strain estimates. *Soil Dynamics and Earthquake Engineering*, 16: 445–457.

Zerva A. (2009) Spatial variation of seismic ground motions. Modeling and engineering applications. CRC Press, Boca Raton.